Photodissociation Dynamics of ArNO Clusters†

Bradley F. Parsons and David W. Chandler*

Sandia National Laboratories, Combustion Research Facility, Livermore, California 94550

Elizabeth C. Sklute, Sissi L. Li, and Elisabeth A. Wade

Department of Chemistry and Physics, Mills College, Oakland, California 94613

Received: June 14, 2004; In Final Form: July 29, 2004

We have investigated the dissociation dynamics of the ArNO van der Waals molecule near 225 nm. This photon energy excites ArNO as much as 400 cm^{-1} above the photodissociation threshold, producing Ar + NO(A $^2\Sigma^+$,v=0,N=0−12). In the first series of experiments, we deduce the population of rotational levels produced in NO(A) during photodissociation of ArNO with resonance enhanced multiphoton spectroscopy (REMPI) through the E-state. The rotational state distributions show anomalous nonstatistical behavior peaking near high N states. This behavior is consistent with the rotational rainbow effects observed by others with the maximum rotational quantum number proportional to the square root of the available energy. In the second experiments, 225 nm photons sequentially dissociate ArNO and then nonresonantly ionize the NO(A) products, which we observe using velocity-mapped ion imaging. The ion images display rings corresponding to the production of different rotational states of NO(A) during dissociation. We measure the appearance threshold for products from dissociation of ArNO to produce NO(A,N=0) as 44291 ± 2 cm^{-1}. Finally, we observe the contribution of hot bands to the rotational state distribution.

I. Introduction

van der Waals complexes have attracted significant interest in the last several decades. ArNO is of particular interest as a benchmark for the interaction of a closed shell atom with an open shell diatom and has been the subject of extensive experimental[1−8] and theoretical[9−13] interest. The interactions of Ar and NO have been studied thoroughly in dynamic[1,3−5] and spectroscopic[2,5,7] studies of the bound complex. On the basis of its spectroscopy Mills et al. determined the structure of the ArNO to be nearly T-shaped with a Jacobi bond angle of 85°.[1]

Using 1+1 REMPI via the NO(F←A) transition, Sato et al. extracted the rotational distributions of NO(A) produced during the photodissociation of ArNO 200−500 cm^{-1} above the dissociation threshold for excited-state NO production.[2] From the appearance of NO(A) rotational states as a function of photon energy, they were able to determine an upper limit for the dissociation energy (D_0'') of ArNO(X) as 88 cm^{-1}:

$$D_0'' \leq h\nu + E_{int} - \nu_{00,NO} - E_{max}(N) \qquad (1)$$

where $h\nu$ is the energy of the photolysis laser pulse, $E_{max}(N)$ is the maximum rotational energy of the NO(A) photoproduct, and $\nu_{00,NO}$ is the transition energy for NO(A,v'=0,N'=0) ← NO(X,v''=0,N''=0). This upper limit of 88 cm^{-1} assumed that ArNO($\tilde{X}$) had no initial internal energy, $E_{int} = 0$.

Sato et al. also observed anomalies in the rotational distribution of the NO(A). These rotational state distributions were not statistical, but instead the distributions consistently exhibited two sharp peaks at high rotational quantum numbers that result from the anisotropy of the potential for the heteronuclear molecule-atom system. They found that the rotational quantum number of each of the rainbow states, N_{max}, was proportional to the square root of the available energy.

The 1+1′ REMPI spectrum of nascent ArNO has been measured by several groups[3−5] and the $\nu_{00,ArNO}$ transition energy for ArNO($\tilde{A}$,v'=0,J'=0) ← ArNO($\tilde{X}$,v''=0,J''=0), is in the range of $\nu_{00,ArNO}$ = 44242−44244.5 cm^{-1}. Furthermore, Monti et al.[5] observed hot bands at 15, 21, and 27 cm^{-1} below $\nu_{00,ArNO}$. These hot bands make a significant contribution to the observed ArNO REMPI spectrum; the integrated intensity of the hot bands is between 20 and 35% of the intensity of the ArNO($\tilde{A}$,v'=0,J'=0) ← ArNO($\tilde{X}$,v''=0,J''=0) transition.

Taken together, the well-known values of $\nu_{00,NO}$ = 44200.7 cm^{-1}, D_0'', and $\nu_{00,ArNO}$ allow for a determination of the dissociation energy for the ArNO($\tilde{A}$). Figure 1 gives a cartoon of the ground and excited state. It can be seen that

$$\nu_{00,ArNO} + D_0' = \nu_{00,NO} + D_0'' \qquad (2)$$

where D_0' is the dissociation energy for ArNO($\tilde{A}$). Upon substitution, eq 2 gives D_0' = 46 cm^{-1}. However, REMPI spectroscopy on ArNO has shown evidence of rovibrational states more than 46 cm^{-1} (=D_0') above $\nu_{00,ArNO}$. The existence of excited-state resonances above D_0' has been explained by a ∼25 cm^{-1} exit barrier resulting from a shape resonance in the dissociation channel on the ArNO($\tilde{A}$) potential energy surface.[3]

We note that NO(A) $^2\Sigma^+$ belongs to the Hund's case b angular momentum coupling scheme where the spin angular momentum is uncoupled from the internuclear axis. The good quantum number for the NO (A) electronic state is $N = J \pm {}^1/_2$.[14] The NO E-state also belongs to Hund's case b coupling scheme. Therefore, the rotational energy for both the A and E states of NO are given as $E_{rot} = B_e N(N + 1)$ (N = 0, 1, 2, ...).

In this study, we use two techniques to investigate the dissociation dynamics of ArNO dimers from threshold to ∼400

† Part of the special issue "Tomas Baer Festschrift".

10.1021/jp047433z CCC: $27.50
Published on Web 10/09/2004

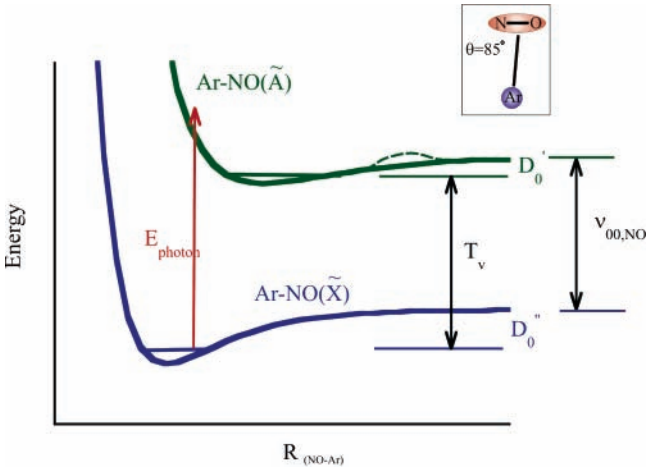

Figure 1. Schematic diagram of the ArNO($\tilde{X}$) state and the ArNO($\tilde{A}$) state. These experiments are performed using 225 nm photons (E_{photon}) near and just above the dissociation threshold on the excited-state D_0''. $\nu_{00,ArNO}$ represents the lowest energy transition between ArNO($\tilde{X}$) and ArNO($\tilde{A}$) whereas $\nu_{00,NO}$ represents the NO(A←X) threshold and D_0' the van der Waals well depth in the ground state. The green dashed curve indicates the possible presence of an exit barrier on the excited state. The inset shows the equilibrium geometry of ArNO($\tilde{X}$). We note that van der Waals molecules such as this are typically floppy and sample a large range of geometries about the equilibrium geometry.

cm^{-1} above threshold. In the first approach, we perform a pump−probe type experiment where a single 225 nm photon dissociates the ArNO dimer followed by 1+1 REMPI of the NO(A) photoproducts through the NO(E) intermediate state. Analysis of the REMPI experiments yields the NO(A) rotational state distribution following dissociation of ArNO. In the second set of experiments, we use velocity-map ion imaging to observe the NO(A) products formed by the dissociation of the dimer from threshold to ~200 cm^{-1} above the threshold. For the imaging experiments, a single laser is used to dissociate the dimer and then nonresonantly ionize the NO(A) products. Analysis of the ion images allows for a confirmation of the energetic threshold for NO(A) production and an investigation into the height of the reverse barrier in the exit channel.

Velocity mapped ion imaging[15] is a technique for the measurement of slow ion velocities perpendicular to the time-of-flight (TOF) axis of a TOF mass spectrometer. Tomas Baer's group pioneered[16] related techniques to measure slow velocities of ions along the TOF axis. These measurements allowed them to determine the kinetics of ion dissociation. Presently, the Baer group has adopted the velocity mapping technique to improve the collection efficiency of zero kinetic energy electrons.[17] We provide details of the experiments in section II and describe the results of the experiments in section III. In section IV.A, we determine the dissociation energy of the ground and excited state using the observed translational energy distributions as a function of photon energy and the threshold for appearance of NO(A) observed in all of our images. In section IV.B, we determine the rotational state distribution of NO(A) following dissociation. The observed rotational state distribution and the change in the distribution as a function of available energy is related to the rotational rainbow phenomena observed previously.[2] We provide brief conclusions on our experiments in section V.

II. Experimental Section

A. REMPI Spectroscopy. We perform these experiments using a ~225 nm photolysis photon from a frequency stabilized dye laser (SpectraPhysics Sirah, Coumarin 450) pumped by an Nd:YAG laser (Coherent Infinity, 2.5 ns pulse). We determine the rotational state distribution of NO (A) via (1+1) REMPI using the E←A transitions near 600 nm.[18] We obtain REMPI probe photons from an Nd:YAG (SpectraPhysics, PRO-290−30, 9 ns pulse) pumped dye laser (Lambda Physik Scanmate 2, Rhodamine B). The unfocused laser pulses propagate coaxially into the scattering region and intersect a molecular beam at a right angle. For these measurements, the molecular beam consists of ~2% NO seeded in Ar expanded at a backing pressure of ~2 atm through a home-built piezoelectric valve[19] (750 μm orifice) and a single skimmer (Beam Dynamics, 800 μm orifice). We observe no significant contribution from higher order clusters in the mass spectrum. We discuss the possibility for the formation of NO(A) from higher order clusters below in section IV.C. During these experiments, the pump laser is held at a fixed photolysis wavelength while the probe laser is scanned in frequency. The time delay between pump pulse, probe pulse, and the gas pulse is controlled using a digital delay generator (Stanford Research Systems, DG-535).

For these experiments, we use a Wiley−McLaren mass spectrometer to project NO^+ onto a stack of two microchannel plates mounted in a chevron configuration. The second microchannel plate couples to a phosphor screen. The output of the phosphor screen is imaged onto a photomultiplier tube whose output is amplified before integration with a boxcar (Stanford Research Systems, SR 250) and then stored on a PC.

B. Photofragment Ion Imaging Experiments. The imaging experiments are performed using a molecular beam system which has been described elsewhere[20] For these experiments, 2% NO seeded in Ar is expanded through a solenoid valve (General Valve Series 9, 700 μm orifice) with a backing pressure of ~2 atm resulting in a beam temperature of 5−10 K. The molecular beam is skimmed once (Beam Dynamics, 650 μm orifice) and crossed with a ~225 nm laser beam, which photolyzes ArNO to produce Ar + NO(A). NO(A) is then nonresonantly ionized by absorption of a second 225 nm photon to produce NO^+, which is accelerated through a Wiley−McLaren time-of-flight mass spectrometer. As above NO^+ (m/e = 30) is mass-selected and projected onto a 2-D position sensitive detector. We record the NO^+ position by imaging the output of the phosphor using a CCD camera (LaVision, Imager 3) to give the final velocity-mapped ion image. The individual ion images are averaged between 1 and 10 min.

The individual images show ring structures corresponding to rotational states of the NO(A) photoproducts. To confirm that the rings we observed result from the ArNO dimer and not from the NO dimer, a NO/He mixture was also expanded in the molecular beam system. This gas mixture produces HeNO dimers that we photolyze near 225 nm. Following dissociation of HeNO, smaller rings corresponding to a smaller recoil velocity appear in the image. The rings from dissociation of HeNO have a smaller velocity due to conservation of energy and momentum in the center-of-mass because a 30 amu particle recoils from a 4 amu particle.

To convert the ion images to energy distributions, the apparatus is calibrated using the previously determined photolysis of O_2 at 225.6 nm.[21] From this photolysis, the magnification factor of the system is determined as 1.22 ± 0.01. Finally, the individual ion images where inverse-Abel transformed using the BASEX program.[22] We generate the recoil kinetic energy distribution directly from the center-of-mass velocity distribution accounting for the appropriate transformation Jacobian.[23]

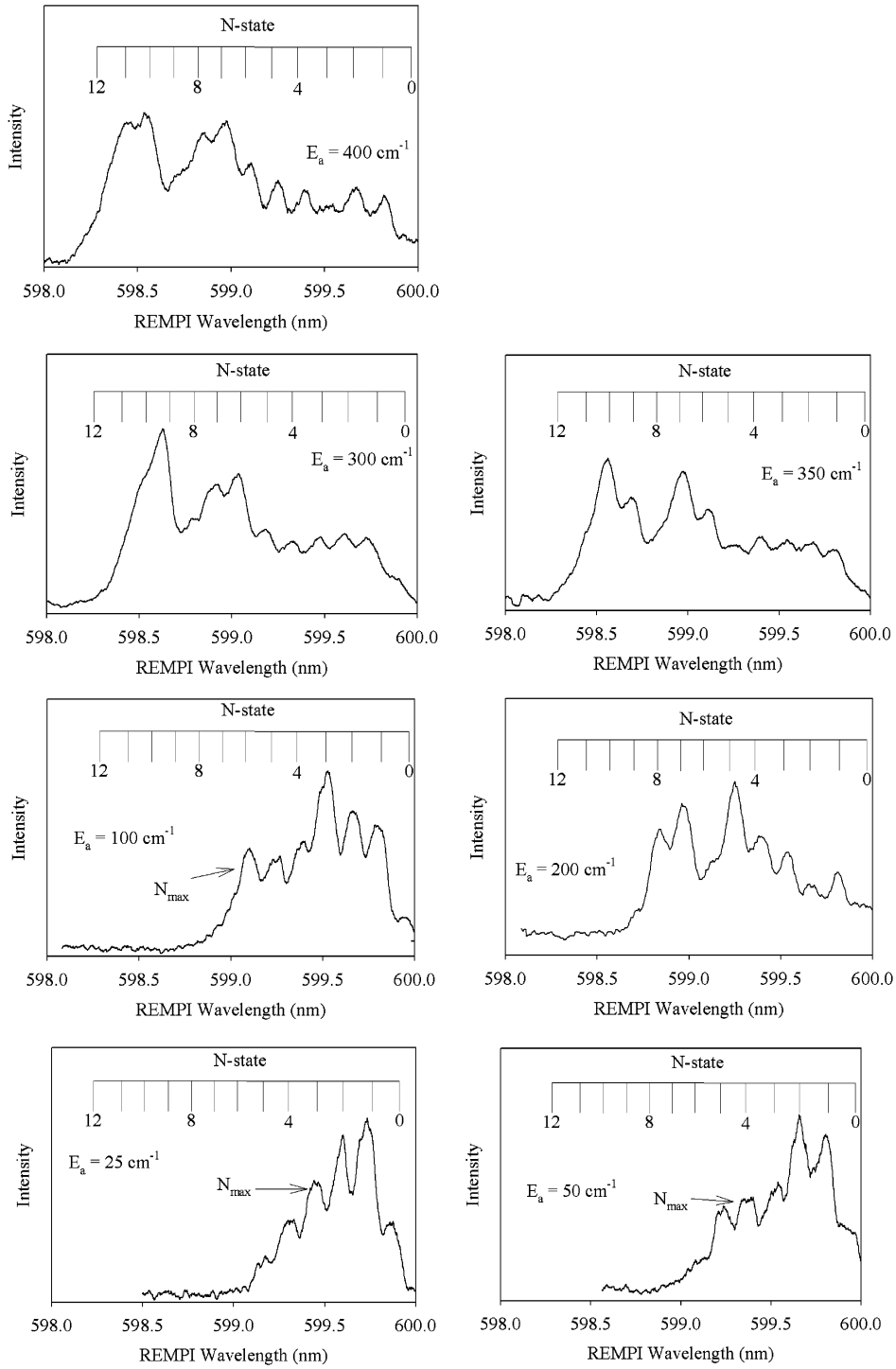

Figure 2. Typical REMPI spectra for ArNO at the specified energy above the barrier to dissociation, E_a.

III. Results

A. REMPI Spectroscopy. Figure 2 shows the observed R-branch of the NO E←A REMPI spectrum at several excitation energies above the threshold for NO(A) production from ArNO (E_a = available energy). We determine the rotational state distribution from the REMPI spectrum by fitting the individual rotational transitions to a Gaussian line shape using the appropriate NO spectral constants.[14] The coefficients of the Gaussian line shapes give the weight for the particular N state in the rotational state distribution. We show the maximum N state, N_{max}, for each excitation energy with a vertical arrow. The REMPI spectrum with $E_a < 100$ cm^{-1} show significant contribution from hot bands as evidenced by the observation of energetically inaccessible rotational states. For $E_a > 100$ cm^{-1}, we do not observe significant contribution from hot bands from the observation of energetically inaccessible rotational states. The lack of hot bands contributing to energetically inaccessible rotational states for $E_a > 100$ cm^{-1} results from the increased spacing between successively higher N states. We point out that the highest energy hot band observed by Monti et al. was 27 cm^{-1}.[5] The energetic spacing between $N = 7$ and $N = 8$ is $\sim$32 cm^{-1}. Therefore, when the excitation photon energy is at the energetic threshold for formation of NO (A,N=7), hot bands cannot contribute enough energy to form $N \geq 8$. However, hot bands may yet contribute to the population of all lower N states.

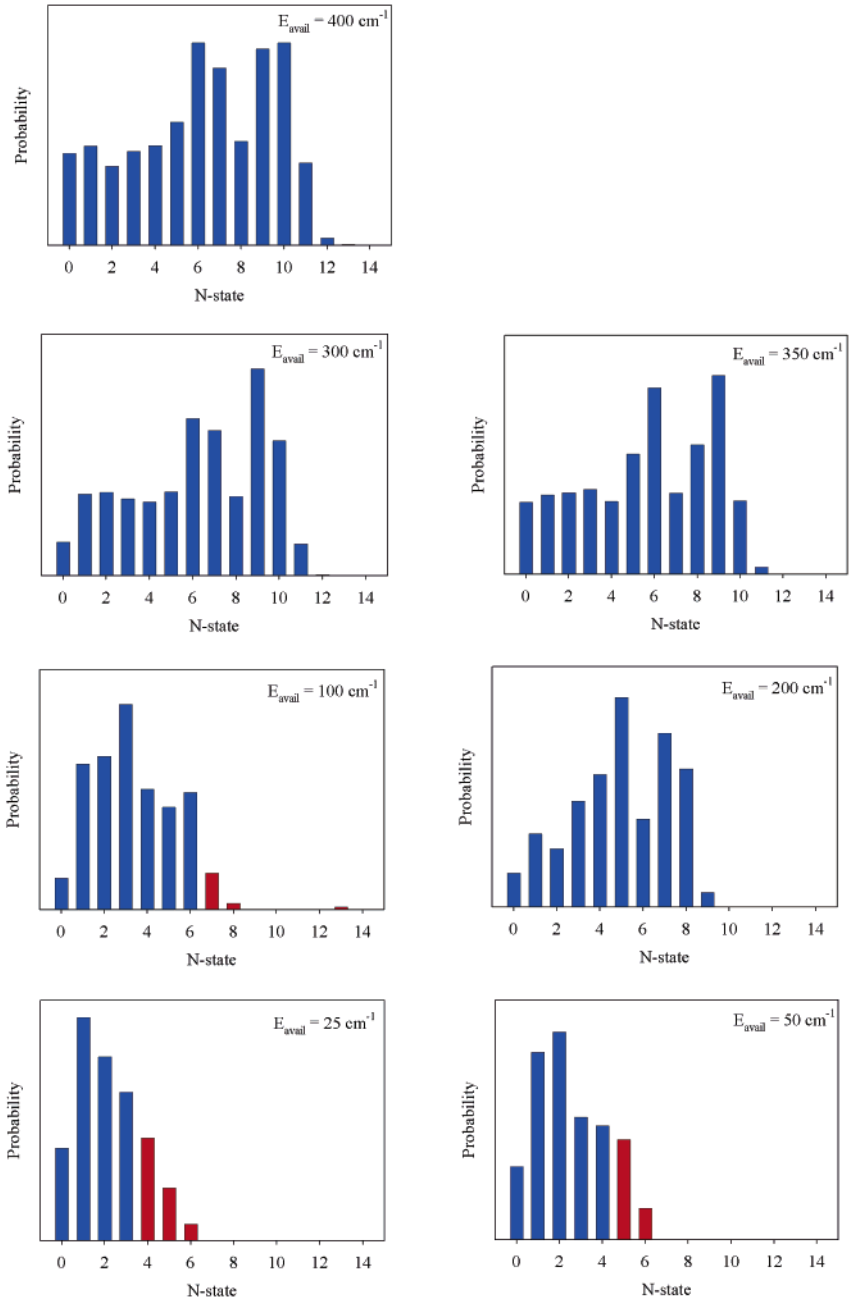

Figure 3. NO(A) rotational distribution for photodissociation of the ArNO dimer at the specified excitation energy. These state distributions were derived by fitting the spectra obtained in the REMPI experiments.

Figure 3 shows a histogram of the NO(A) rotational state distribution for dissociation energies derived from the NO E←A REMPI spectrum. Only the data from the R-branch from the REMPI spectrum are used to derive these distributions because only the R-branch samples NO(A,N=0). The blue bars in the histogram represents rotational states nominally available for a given photolysis wavelength, and the red bars indicates the rotational states that must result from excitation of ArNO hot bands. The influence of hot bands in the individual rotational state distributions is clearly evident at energies close to the dissociation threshold. As the photolysis energy increases, the contribution of hot bands to the rotational state distribution, as observed through the formation of energetically forbidden rotational states, decreases dramatically. However, as mentioned previously, hot bands can contribute to all energetically allowed rotational states at a given photolysis energy.

B. Photofragment Ion Imaging. A typical ion image following the photolysis of the ArNO dimer appears in Figure 4; the spot in the center of the image is due to nonresonant ionization of nascent NO(X $^2\Pi_{1/2}$) in the molecular beam. The NO(A) image from the dimer dissociation shows no recoil anisotropy. The lack of anisotropy may result from dissociation of ArNO after several rotational periods which scramble the original alignment of the excited dimer. The analysis proceeds by performing an inverse Abel transform on the individual images. The inverse-Abel transform reconstructs the three-dimensional velocity distribution from its projection, which results when the product sphere is crushed onto the 2-D detector. The center-of-mass (CM) velocity for the photofragments may then be converted into a CM recoil kinetic energy distribution. As discussed above, the CM velocity distributions are converted to CM recoil kinetic energy distribution accounting for the

TABLE 1

	McQuaid et al.[a]	Tsuji et al.[b]	Casavecchia et al.[c]	Thuis et al.[d,e]	present work
D_0'' (ArNO $\tilde{X}$), cm^{-1}		88	96 ± 4.6	73−96	90 ± 2
D_0' (ArNO $\tilde{A}$), cm^{-1}	43	44			
$E_{\text{reverse barrier}}$ (ArNO $\tilde{A}$), cm^{-1}		25			

[a] Reference 3. [b] Reference 7. [c] Reference 8. [d] Reference 28. [e] The range in D_0'' refers to the fit from several different models presented. [f] The current experiments cannot directly determine the presence of an exit barrier. We are considering future experiments to directly investigate the height of such a barrier.

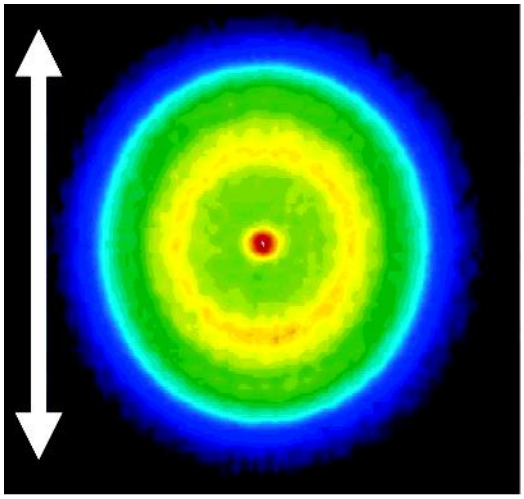

A.

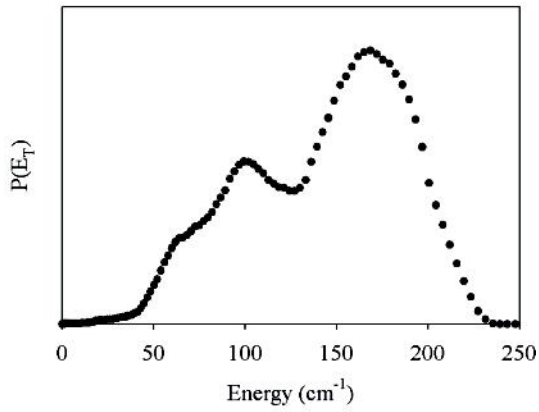

B.

Figure 4. Typical ion image for NO(A) produced following photodissociation of the ArNO dimer excited at ~224.75 nm ($E_{ph} = 44495$ cm^{-1}).

transformation Jacobian.[23] At the bottom of Figure 4 we show the recoil kinetic energy distribution, $P(E_T)$, derived from the ion image at the top of Figure 4.

IV. Discussion

A. Dissociation Threshold and Barrier. The threshold for photodissociation of the ArNO dimer can be measured by determining the energy for onset of the first ring in the ion imaging experiments; we determine the threshold for appearance of NO(A) products to be 44291 ± 2 cm^{-1}. Interpreting this as a dissociation threshold with no barrier and using the known value of $\nu_{00,NO} = 44201$ cm^{-1}, we find the well depth on the ground state to be $D_0'' \sim 90 \pm 2$ cm^{-1}, in good agreement with previous observations, as summarized in Table 1.

At the appearance threshold we observe distinct rings corresponding to NO(A,N=0) with as little as 2 cm^{-1} of recoil translational energy. Smaller rings corresponding to NO(A,N=0) may be present, but we are unable to resolve any because they merge into the central beam spot. However, we can consider if a significant (~25 cm^{-1}) barrier in the excited may be consistent with small product translational energies. To do this, we assume that an excited-state exit barrier exists with a height of ~25 cm^{-1}. In this case, dimers that are rovibrationally cold in the ground state lack sufficient energy to dissociate but dimers that are excited from hot bands (we discuss these in section IV.C) may have sufficient energy to dissociate. Indeed, the highest hot band previously observed is 27 cm^{-1}.[5] Of course, dimers resulting from hot band excitation have enough energy to form NO(A,N=0−3). Tsuji et al. observed the production of NO(A,N=1−3) using action spectroscopy. We note that their results do not show evidence of dimer hot bands. Their spectra show that the production of $N = 1$ and $N = 2$, which form by tunneling through a shape resonance in the excited state, essentially shuts off once NO(A,N=3) is energetically allowed. Thus, near threshold dissociation appears to favor formation of NO(A) in the highest energetically allowed rotational state. Of course, the formation of rotationally hot NO(A) at threshold requires minimal energy release, resulting in what appears to be a beam spot. This observation is consistent with either a barrierless dissociation with no significant contribution from hot bands or an approximately 25 cm^{-1} barrier and hot band dissociation leading exclusively to rotationally hot products. We are considering future experiments to determine if such a barrier does exist on the ArNO excited state.

B. Rotational State Distributions. The REMPI spectra shown in Figure 2 provide a direct measure of the rotational state distribution. As an independent check of the rotational states distributions, we fit the recoil kinetic energy distribution, $P(E_T)$ derived from our imaging experiments to a sum of Gaussian functions centered at the translational energy of a given rotational state of NO(A):

$$P(E_T) = C_{HB} \exp\{-(T - (E_a + 27))^2/\alpha_1\} + \sum_N C_N \exp\{-(T - E_a + E_N)^2/\alpha_2\} \quad (3)$$

The first term in eq 3 accounts for the contribution of hot bands to the $P(E_T)$. C_{HB} weights this term and α_1 gives the width for the fitting function. The energy of the hot bands is chosen as the maximum observed by Monti et al., 27 cm^{-1}.[5] In eq 3, $E_a = E_{photon} - D_0'' - \nu_{00,NO}$ is the available energy that may be partitioned into translation and product rotation, assuming $E_{int}(ArNO) = 0$. E_N is the energy of a given NO(A) N state, and C_N is the weighting of that particular N state to the total $P(E_T)$. The same width parameter, α_2, is used for each N state. In Figure 5A we show the fit to our $P(E_T)$ derived from the image in Figure 4. The resulting rotational state distribution that fits the $P(E_T)$ appears in Figure 5B as open triangles along with the rotational state distribution derived from the REMPI spectrum taken with $E_a = 200$ cm^{-1}, solid squares.

Inspection of the rotational state distributions from our experiments, shown in Figure 5, reveals several interesting

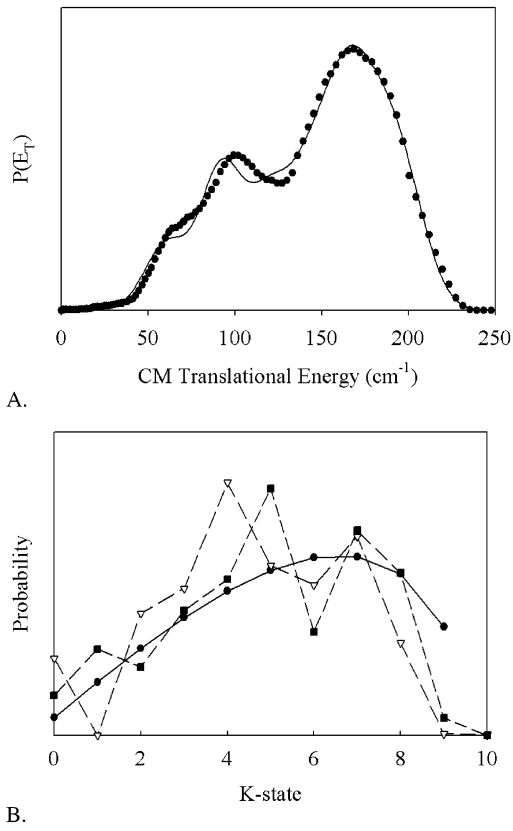

Figure 5. (Top) recoil kinetic energy distribution and the fit to the $P(E_T)$ as described in the text. (Bottom) derived rotational state distribution from the fit to the $P(E_T)$ (open triangle) along with the rotational state distribution exctracted from REMPI spectroscopy experiments at $E_a = 200$ cm^{-1} (solid squares) and the rotational state distribution predicted by a Prior distribution function (solid circles).

features. First, increasing the available energy allows formation of higher NO(A) rotational states as the ArNO dimer dissociates. However, both experimental rotational state distributions in Figure 5B show a curious peaked structure for high N states and are distinctly nonstatistical. To demonstrate, we calculate the Prior distribution for dissociation of dissociation of ArNO at $E_a = 200$ cm^{-1}. The Prior distribution function gives a statistical rotational distribution appropriate for photodissociation when only one fragment has available rotational states.[24] The Prior distribution is represented by circles in Figure 5B. The REMPI and the imaging experiments agree fairly well in the general structure of the rotational state distribution, and both predict the second peak rotational state correctly. On the other hand, the statistical distribution does not reproduce the general structure of the experimentally measured rotational state distributions.

Sato et al. observed a similar distribution for the rotational states of NO(A) produced by dissociation of ArNO at 200−500 cm^{-1} above threshold, with two peaks appearing at high rotational quantum numbers. They found that the peak rotational state depends linearly on the square root of E_a, $N_{max} \propto \sqrt{E_a}$. This was interpreted as resulting from a rotational rainbow effect as described by others for the fragmentation of systems as HeI_2 and formaldehyde.[25−27] Schinke[27] interpreted the rotational state distribution of CO and H_2/D_2/HD from formaldehyde using a simple model where the probability of a given final rotational state is

$$P(j) = \left|\frac{\sin \gamma_v}{dJ(\gamma)/d\gamma}\right| |\phi_\gamma(\gamma_v)|^2 \qquad (4)$$

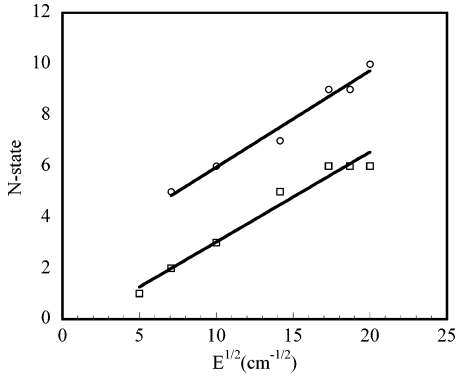

Figure 6. Maximum observed NO(A) rotational states vs $\sqrt{E_a}$ for ArNO. The plot gives a straight line in agreement with the predicted rotational rainbow behavior. We plot the behavior of both the high rotational peak (open squares) and the low rotational peak (open circles) along with lines to guide the eye.

where $J(\gamma)$ is termed the excitation function and depends on the internal Jacobi coordinate, γ, and the function $\phi(\gamma)$ is a weighting function. The observed rotational state distribution is a projection of this product onto the rotational quantum number. The term rotational rainbow refers to the fact that for one particular angle, γ_0, $J(\gamma)$ maps to a particular value of the rotational angular momentum, J_{max}. However, for all values of the rotational angular momentum below J_{max}, two angles (one above γ_0 and one below γ_0) map $J(\gamma)$ to the same value of the angular momentum. Thus, as γ_0 is approached from above and below, the mapping of $J(\gamma)$ coalesces to a single value of the rotational angular momentum, leading to a rainbow effect similar to that observed in bimolecular scattering. Classically, the excitation function is proportional to the square root of the reduced mass and the energy. In the case of HDCO fragmentation[27] near 29500 cm^{-1}, the predicted HD rotational state distribution shows two peaks at higher quantum numbers, resulting from the anisotropy of the potential similar to that observed by Sato et al.[2]

Anisotropy in the structure of the dimer, including any distortion from a T-shaped geometry, creates an anisotropy in the potential energy surface so the dissociation may take place through two distinct exit channels. Both exit channels generate the same chemical products with different internal states. For HDCO, when the CO recoils primarily from the H side, the distribution peaks at a different rotational state than when it recoils from the D side. On the other hand, dissociation of a homonuclear−diatomic dimer such as Ar·I_2 should result in a single peak in the rotational state distribution.

The peaked structure in our rotational state distribution could result from the anisotropy of the ArNO potential. In Figure 6 we plot the two maxima of the rotational state distribution for ArNO as a function of the square root of available energy. The plot shows good agreement with the prediction $K_{max} \propto \sqrt{E_a}$, for both observed peaks, as is consistent with the rotational rainbow effect observed by Sato et al.

C. Contributions from Hot Band and Higher Order Clusters. Our observation of the dissociation threshold from the ion imaging experiments agrees with that found in previous experiments investigating photodissociation of the dimer to product NO(A)[5] and in bimolecular scattering experiments of NO(X) + Ar.[8,28] If excitation near the threshold occurred from hot bands, then the observed energetic threshold would be larger than that observed previously by the energy of the hot bands because $E_a = E_{ph} + E_{HB} - D_0''$. Hence, the agreement we observe for the energetic threshold is consistent with either hot

bands are not excited near the threshold or the dissociation of the 27 cm^{-1} hot band over an approximately 25 cm^{-1} barrier gives the same threshold behavior. However, the REMPI spectra taken between 25 and 100 cm^{-1} above threshold, Figure 2, and the rotational state distribution, Figure 3, reveal NO(A) *N* states that are energetically inaccessible. The nominally energetically forbidden *N* states must result from hot band excitation 25 cm^{-1} above the dissociation threshold. Therefore, the hot band absorption is weak near the energetic threshold. This surprising change in the hot band absorption may be due to changes in the Franck−Condon factors near the threshold for dissociation.

On the other hand, the high energy REMPI spectra (E_a > 100 cm^{-1}) do not show any significant contribution from hot bands for the highest rotational states. Likewise, Sato et al.[2] observe a similar value for D_0'' using F←A NO REMPI spectroscopy 200−500 cm^{-1} above threshold. Well above threshold, hot bands do not contribute to the highest energetically allowed NO *N* states. This effect may result from some dynamical constraint at higher internal energies. Therefore, the hot band absorption appears to be weak at the energetic threshold for production of NO(A) through photodissociation of ArNO. However, as the available energy increases, hot bands show considerable contribution to the photodissociation dynamics up to $E_a \sim 100$ cm^{-1}. As the available energy is further increased, the contribution to hot bands seem to contribute less to the production of energetically inaccessible rotational states due to the increased spacing between progressively higher *N* states. The curious absorption behavior of hot bands near the energetic threshold for production of NO(A) could result from rapid change in the magnitude of the Franck−Condon factors in this energetic region

Finally, we point out the recoil translational energy distributions observed in the ion imaging experiments typically extend beyond the energetic limit. Two possible effects may explain this observation. First, the hot band contribution may be large for low *N* states (larger recoil kinetic energies). This would shift the tail for the $P(E_T)$ to larger energies. Indeed, the $P(E_T)$ shown in Figure 5A for excitation 200 cm^{-1} above the energetic threshold extends to about 225 cm^{-1} in good agreement with the most energetic hot band observed previously.[5]

An alternative explanation for the high energy tail observed in the $P(E_T)$ is the possibility for contribution of NO produced during the dissociation of higher order clusters. i.e., Ar_nNO (n > 1). We now address how cluster dissociation would influence the high energy limit for the $P(E_T)$. As discussed above, the $P(E_T)$ in Figure 5A is derived assuming that the NO fragment is momentum matched to Ar (mass = 40). If, instead, some NO fragments are momentum matched to Ar_n (n > 1), then for the same amount of relative translational energy, the CM velocity for these NO will be greater owing to the increased mass of the partner Ar_n fragment. In Figure 5A, the available energy is 200 cm^{-1}. If all of the available energy is partitioned into relative translation, then the observed CM velocity for NO would be

$$V_{NO} = 302 \text{ m/s(ArNO)} \quad (5a)$$

$$V_{NO} = 342 \text{ m/s } (Ar_2NO) \quad (5b)$$

where the upper velocity refers to NO momentum matched with Ar and the lower velocity refers to NO momentum matched with Ar_2. However, because our $P(E_T)$ is derived by assuming NO momentum matched to Ar (mass = 40), then if we were to record NO fragments with a CM velocity of 342 m/s, we would over predict the CM translational energy to be $E_T = 257$ cm^{-1} (because our momentum matching assumption would be incorrect). To estimate the energetic limit for cluster dissociation, we have assumed that the dissociation energy in the ground state and the excited state for higher order clusters is the same as for the dimer. Furthermore, we have ignored the internal mode for Ar_2 and possible effects of three body dissociation. However, this energetic limit $E_T = 257$ cm^{-1} does extend well beyond the limit of the $P(E_T)$ shown in Figure 5A, which suggests that higher order clusters do not contribute significantly to the observed signal. Furthermore, we do not observe any higher order clusters in the mass spectrum during the experiment.

V. Conclusions

The ArNO dimer is photodissociated to produce Ar + NO(A) with 0 to 400 cm^{-1} of recoil energy, and the NO(A) is then nonresonantly ionized and observed using velocity-mapped ion imaging. The ion images display distinctive ring patterns that are assigned to rotational states of NO(A). The threshold for observation of these rings is measured at 44291 ± 2 cm^{-1}, which under the assumption that hot bands do not contribute to the observed signal, gives an upper limit for the dissociation energy of ArNO($\tilde{X}$) and ArNO($\tilde{A}$) of 90 ± 2 and 46 ± 2 cm^{-1}, respectively. Lower limits, based on estimates for the maximum internal energy of the ArNO dimer prior to dissociation, are also determined to be 84 ± 3 and 40 ± 3 cm^{-1}, respectively.

Rotational state distributions for NO(A) are extracted from the 1+1 REMPI spectrum of NO(A) at several excitation energies. We fit the derived $P(E_T)$ to a function form that gives a rotational state distribution in fair agreement with that observed in the REMPI experiments. These rotational state distributions exhibit a rotational rainbow effect, with the rotational quantum number of the maximum rotational state proportional to the square root of the available energy.

Finally, we observe the energetic threshold for NO(A) state production. This threshold is consistent with a barrier and hot band absorption or no barrier and no hot band absorption. As the excitation energy increases, the contribution from hot bands to the largest observed *N* states may decrease due to some dynamical constraint on the excited-state potential energy surface. However, a complete understanding of this experiment requires high-quality calculations for the excited-state potential energy surface.

Acknowledgment is made to the Donors of the American Chemical Society Petroleum Research Fund, for partial support of this research. S.L.L. was partially supported by a Barrett Undergraduate Research Award. We thank Millard Alexander and Reinhard Schinke for helpful discussions. We also thank Mark Jaska for technical assistance and Doug Wade for programming assistance. We acknowledge the financial support from the Department of Energy Office of Basic Energy Sciences, Division of Chemical Sciences, Geosciences, and Biosciences. Sandia is a multiprogram laboratory operated by Sandia Corp., a Lockheed Martin Co., for the United States Department of Energy's National Nuclear Security Administration under contract DE-AC04-94AL85000.

References and Notes

(1) Mills, P. D. A.; Western, C. M.; Howard, B. J. *J. Phys. Chem.* **1986**, *90*, 4961.

(2) Sato, K.; Achiba, Y.; Nakamura, H.; Kimura, K. *J. Chem. Phys.* **1986**, *85*, 1418.

(3) McQuaid, M. J.; Lemire, G. W.; Sausa, R. C. *Chem. Phys. Lett.* **1994**, *227*, 54.

(4) Bush, A. M.; Dyke, J. M.; Mack, P.; Smith, D. M.; Wright, T. G. *J. Chem. Phys.* **1998**, *108*, 406.

(5) Monti, O. L. A.; Cruse, H. A.; Softley, T. P.; Mackenzie, S. R. *Chem. Phys. Lett.* **2001**, *333*, 146.
(6) Langridge-Smith, P. R. R.; Carrasquillo, E. M.; Levy, D. H. *J. Chem. Phys.* **1981**, *74*, 6513.
(7) Tsuji, K.; Shibuya, K.; Obi, K. *J. Chem. Phys.* **1994**, *100*, 5441.
(8) Casavecchia, P.; Lagana, A.; Volpi, G. G. *Chem. Phys. Lett.* **1984**, *112*, 445.
(9) Green, S.; Zare, R. N. *Chem. Phys.* **1975**, *7*, 62.
(10) Nielson, G. C.; Parker, G. A.; Pack, R. T. *J. Chem. Phys.* **1977**, *66*, 1396.
(11) Alexander, M. H. *Chem. Phys.* **1985**, *92*, 337.
(12) Alexander, M. H. *J. Chem. Phys.* **1993**, *99*, 7725.
(13) Alexander, M. H. *J. Chem. Phys.* **1999**, *111*, 7426.
(14) Herzberg, G. *Spectra of Diatomic Molecules*; D. van Nostrand Co. Inc.: Princeton, NJ, 1950.
(15) Chandler, D. W.; Houston, P. L. *J. Chem. Phys.* **1987**, *87*, 1445.
(16) Duffy, L. M.; Keister, J. W.; Baer, T. *J. Phys. Chem.* **1995**, *99*, 17862.
(17) Sztaray, B.; Baer, T. *Rev. Sci. Instrum.* **2003**, *74*, 3763.
(18) Naitoh, Y.; Fujimura, Y.; Honma, K.; Kajimoto, O. *Chem. Phys. Lett.* **1993**, *205*, 423.
(19) Proch, D.; Trickl, T. *Rev. Sci. Instrum.* **1989**, *60*, 713.
(20) Parsons, B. F.; Chandler, D. W. *J. Phys. Chem. A* **2003**, *107*, 10544.
(21) Eppink, A. T. J. B.; Parker, D. H. *Rev. Sci. Instrum.* **1997**, *68*, 3477.
(22) Dribinski, V.; Ossadtchi, A.; Mandelshtam, V. A.; Reisler, H. *Rev. Sci. Instrum.* **2002**, *73*, 2634.
(23) Warnock, T. T.; Bernstein, R. B. *J. Chem. Phys.* **1968**, *49*, 1878.
(24) Baer, T.; Hase, W. L. *Unimolecular Reaction Dynamics*, 1st ed.; Oxford University Press: New York, 1996.
(25) Schinke, R. *Chem. Phys. Lett.* **1985**, *120*, 129.
(26) Segev, E.; Shapiro, M. *J. Chem. Phys.* **1983**, *78*, 4969.
(27) Schinke, R. *J. Chem. Phys.* **1986**, *84*, 1487.
(28) Thuis, H. H. W.; Stolte, S.; Reuss, J.; van den Biesen, J. J. H.; van den Meijdenberg, C. J. N. *Chem. Phys.* **1980**, *52*, 211.